nature physics

Article

https://doi.org/10.1038/s41567-023-02361-4

Demonstration of a hydrodynamically equivalent burning plasma in direct-drive inertial confinement fusion

Received: 23 February 2023

Accepted: 29 November 2023

Published online: 05 February 2024

Check for updates

V. Gopalaswamy[1,2] ✉, C. A. Williams[1,3], R. Betti[1,2,3], D. Patel[1,2], J. P. Knauer[1], A. Lees[1,2], D. Cao[1], E. M. Campbell[1], P. Farmakis[1,2], R. Ejaz[1,2], K. S. Anderson[1], R. Epstein[1], J. Carroll-Nellenbeck[1], I. V. Igumenshchev[1], J. A. Marozas[1], P. B. Radha[1], A. A. Solodov[1], C. A. Thomas[1], K. M. Woo[1], T. J. B. Collins[1], S. X. Hu[1], W. Scullin[1], D. Turnbull[1], V. N. Goncharov[1], K. Churnetski[1], C. J. Forrest[1], V. Yu. Glebov[1], P. V. Heuer[1], H. McClow[1], R. C. Shah[1], C. Stoeckl[1], W. Theobald[1,6], D. H. Edgell[1], S. Ivancic[1], M. J. Rosenberg[1], S. P. Regan[1], D. Bredesen[1], C. Fella[1], M. Koch[1], R. T. Janezic[1], M. J. Bonino[1], D. R. Harding[1], K. A. Bauer[1], S. Sampat[1], L. J. Waxer[1], M. Labuzeta[1], S. F. B. Morse[1], M. Gatu-Johnson[4], R. D. Petrasso[4], J. A. Frenje[4], J. Murray[5], B. Serrato[5], D. Guzman[5], C. Shuldberg[5], M. Farrell[5] & C. Deeney[1]

Focussing laser light onto the surface of a small target filled with deuterium and tritium implodes it and leads to the creation of a hot and dense plasma, in which thermonuclear fusion reactions occur. In order for the plasma to become self-sustaining, the heating of the plasma must be dominated by the energy provided by the fusion reactions—a condition known as a burning plasma. A metric for this is the generalized Lawson parameter, where values above around 0.8 imply a burning plasma. Here, we report on hydro-equivalent scaling of experimental results on the OMEGA laser system and show that these have achieved core conditions that reach a burning plasma when the central part of the plasma, the hotspot, is scaled in size by at least a factor of 3.9 ± 0.10, which would require a driver laser energy of at least 1.7 ± 0.13 MJ. In addition, we hydro-equivalently scale the results to the 2.15 MJ of laser energy available at the National Ignition Facility and find that these implosions reach 86% of the Lawson parameter required for ignition. Our results support direct-drive inertial confinement fusion as a credible approach for achieving thermonuclear ignition and net energy in laser fusion.

Inertial confinement fusion (ICF)[1,2] uses high power drivers such as lasers[3,4], particle beams or pulsed power[5] to implode millimetre-scale payloads containing fusion fuels such as deuterium (D) and tritium (T) to high densities and temperatures, generating copious fusion reactions. The D+T fusion reaction produces a helium ion (alpha particle) with 3.5 MeV energy and a neutron with 14.03 MeV energy. The alpha particle carries approximately 20% of the fusion energy, providing the main source of plasma self-heating. Laser ICF uses lasers as the

[1]Laboratory for Laser Energetics, Rochester, NY, USA. [2]Department of Mechanical Engineering, University of Rochester, Rochester, NY, USA. [3]Department of Physics and Astronomy, University of Rochester, Rochester, NY, USA. [4]Plasma Science and Fusion Center, Massachusetts Institute of Technology, Cambridge, MA, USA. [5]General Atomics, San Diego, CA, USA. [6]Present address: Focused Energy, Austin, TX, USA. ✉e-mail: vgop@lle.rochester.edu

driving energy source, either by directly illuminating the target (laser direct-drive (LDD))[4] or indirectly via X-rays generated by laser illumination of a high-atomic-number enclosure surrounding the target (laser indirect-drive (LID))[3].

LDD ICF payloads are typically spherical and comprise a cryogenic deuterium–tritium (DT) fuel layer surrounded by an ablator of moderate atomic number ($Z \approx 3$–7), such as a carbon–deuterium polymer, high-density carbon or beryllium. The laser light is incident on the payload surface at intensities ~10^{15} W cm^{-2}, which ablates the surface of the shell and rapidly accelerates (at ~10^{15} m s^{-2}) the remaining payload inward to a velocity between 300 and 600 km s^{-1}. Eventually, the unablated fuel shell converges by a factor of 10–30, amplifying the pressure of the tenuous gas in the interior to the point where the shell begins to decelerate. As it does so, the shell acts as a piston on the interior gas, increasing its temperature to a few keV. This drives mass ablation on the shell's interior as it comes to a halt, forming a low density (30–100 g cm^{-3}) and high temperature (3–7 keV) hotspot, surrounded by a dense (100–1,000 g cm^{-3}) and low temperature (~200 eV) shell. The inertia of this shell is sufficient to confine the high pressure (100–400 Gbar) hotspot for a subnanosecond duration, sufficient time for fusion reactions to occur. If the appropriate conditions[6–10] are met in the stagnated configuration, the alpha particles deposit their energy into the hotspot (alpha heating), leading to a runaway thermal instability known as ignition that substantially amplifies the fusion energy output of the implosion. A key milestone on the path toward ignition is the generation of a 'burning plasma', in which the energy deposited into the hotspot by the alpha particles exceeds the compression work done on the hotspot. The burning-plasma state heralds the transition of the fusion hotspot into a regime where the feedback processes leading to ignition are dominant and thus places a fusion experiment in a region where rapid increases in energy output become possible.

Demonstrating a burning plasma and ignition are important milestones on the path to the high gains ($G = E_{\text{fusion}}/E_{\text{driver}} \gg 1$) necessary for inertial fusion energy, with gains over 100 being a likely requirement for commercial viability. Achieving the burning-plasma state and triggering ignition requires an efficient transfer of energy from the driver to the kinetic energy of the fuel (coupling efficiency $\eta = KE_{\text{fuel}}/E_{\text{driver}}$). The first plasmas with significant alpha heating[11], with a burning plasma[12,13] and with an ignited plasma[14] were reported by researchers at the National Ignition Facility (NIF) using the LID approach to fusion. Owing to the intermediate stage where laser light is converted to X-rays in LID, it has a lower η, 20–25% of that exhibited by LDD[10]. LID targets are also more complex than LDD targets, as LID targets require the fabrication of a metal cylindrical enclosure (typically of gold or other high-atomic-number metal) in which the target must be precisely centred. For commercial inertial fusion energy applications, where minimizing the cost of the driver and targets is of high importance[15], the advantages of LDD make it a more attractive option for carbon-free energy production.

Although the 2.15 MJ NIF is unique in its ability to conduct implosions that can achieve significant alpha heating via LID[11–14], it is not capable of symmetric LDD DT-layered implosion experiments in its present configuration. These experiments are instead carried out on the 30 kJ OMEGA Laser System. Owing to its substantially lower energy, the fusion plasmas created on OMEGA are smaller (to maintain similar energy density, the size of the fusion plasma $R_{\text{fusion}} \approx E_{\text{laser}}^{1/3}$). Consequently, the plasma size is smaller than the mean-free-path λ_α of the alpha particles and meaningful alpha heating cannot occur. Therefore, to assess the progress in LDD on OMEGA, we need to scale the results on OMEGA to the laser energies demonstrated at the NIF. While a variety of approaches of scaling to higher energy facilities have been investigated, the approach used here is a minimal-assumption theory known as hydro-equivalent scaling[16–18].

Hydro-equivalent scaling assumes only that the hotspot conditions demonstrated on OMEGA can be reproduced at larger scales so that any increase in alpha heating is simply a result of the larger size of the implosion. Therefore, in scaling up OMEGA results, the hotspot pressure and shell density are kept constant, the hotspot size is increased, and the hotspot temperature follows the Spitzer thermal-conduction size scaling. The result of the size scaling is robust; the only new physics that needs to be considered is the stopping of alpha particles, which is determined by λ_α. The general agreement of various stopping power models[19] and the success of the various alpha-heating models[6–10] in modelling the onset of the burning plasma and ignition conditions at the NIF[11–14] suggest that models for λ_α are reasonably accurate. The biggest uncertainties in hydro-equivalent scaling arise when connecting the increase in size to the required increase in driver energy, where hydro-equivalent scaling assumes that the coupling efficiency η is scale invariant so that the incident laser energy required scales as the hotspot volume. A detailed discussion on the validity of hydro-equivalent scaling can be found in the Methods, with simulation and experimental results in Extended Data Figs. 1 and 2 and Extended Data Table 1; however, we stress that the hydro-equivalent scaling theory used here does not assert that its results are achievable on the NIF as presently configured.

LDD experiments carried out with cryogenic targets on the 30 kJ OMEGA laser have met several important milestones in recent years. The primary metric of progress in LDD is the increase in the generalized Lawson parameter $\chi_{\text{no}\alpha}$ as parametrized in ref. 6,17,

$$\chi_{\text{no}\alpha} = (\rho R)^{0.61}\left(\frac{0.12Y_{16}}{M_{\text{DT}}^{\text{stag}}}\right)^{0.34}, \quad (1)$$

where ρR, Y_{16} and $M_{\text{DT}}^{\text{stag}}$ are, respectively, the areal density in g cm^{-2}, the yield in units of 10^{16} neutrons and the stagnated DT mass in milligrammes at the time of peak neutron production; $\chi_{\text{no}\alpha} > 0.8$ and 0.96 imply a burning plasma and ignition, respectively. Another metric to measure progress toward ignition is the yield amplification due to alpha heating,

$$\hat{Y} = \frac{Y_\alpha}{Y_{\text{no}\alpha}}, \quad (2)$$

where Y_α is the fusion yield of the implosion and $Y_{\text{no}\alpha}$ is the fusion yield for the same implosion if it did not have alpha heating, that is, where the hotspot is heated only by compression work. $\hat{Y}$ can be determined in simulations by taking the ratio of yields from simulations with and without alpha-heating physics enabled and in experiments using surrogate implosions with substantially reduced or zero deuterium content[7]. $\hat{Y}$ and $\chi_{\text{no}\alpha}$ are closely related as shown in ref. 9; $\hat{Y} \gtrsim 3.5$ implies a burning plasma[9] and $\hat{Y}$ in the range 15–25 implies ignition[8].

In 2016, LDD implosions demonstrated core conditions which when extrapolated to realizable NIF energies would be expected to have $\chi_{\text{no}\alpha} \approx 0.6$ and its yield doubled by alpha heating[17,20] and were expected to produce up to ~125 kJ of fusion energy. In 2019, a data-driven statistical approach was pioneered on OMEGA to enable predictive implosion design[18], which rapidly tripled the fusion yield on OMEGA without seriously compromising the areal density ρR. These implosions were of lower convergence and greater hydrodynamic stability and therefore less demanding than previous designs. When extrapolated to realizable NIF energies, these designs were expected to have $\chi_{\text{no}\alpha} \approx 0.74$, resulting in an expected yield amplification of ~3 due to alpha heating and fusion energies of up to ~500 kJ. Subsequently, this approach was used alongside an innovative low-mode-symmetry[21] and fuel-purity[22] control framework to identify, quantify and mitigate physical degradation mechanisms on OMEGA[23], leading to increased repeatability and control of experiments. A detailed discussion of the Statistical Model can be found in ref. 24.

The current work, along with its companion paper[25] describe the next milestones that have been achieved in LDD. The companion

paper[25] discusses how the energy transfer to the hotspot plasma was optimized on OMEGA to achieve hotspot fuel gain, in which the fusion energy exceeds the internal energy of the hotspot fuel. This work describes how cryogenic experiments on OMEGA have achieved core conditions that hydro-equivalently extrapolate to a burning plasma at achievable incident laser energies. We first show that recent OMEGA implosions have achieved core conditions that reach a burning plasma when scaled hydro-equivalently in size by at least a factor of 3.9 ± 0.10, which requires a driver energy of at least 1.7 ± 0.13 MJ under hydro-equivalent conditions. We then show that, at the maximum realizable NIF energies of 2.15 MJ, these implosions hydro-equivalently increase in size by a factor of 4.2 and therefore extrapolate to a Lawson parameter of 0.86 ± 0.02 with an extrapolated fusion energy output of up to 1.6 ± 0.3 MJ. We then show that these extrapolated conditions are well within the burning-plasma region; we describe the implosion design changes from ref. 18 that enabled this result; and we finish by describing the path toward hydro-equivalent ignition and high gains for LDD.

Demonstration of a scaled burning plasma

A burning-plasma state is achieved when the cumulative alpha heating of the hotspot up to the point of maximum fusion rate E_α exceeds the compression work E_{PdV} done on the hotspot by the imploding shell up to that point[9], so that the burning-plasma parameter Q_α is given by

$$Q_\alpha = \frac{E_\alpha}{E_{PdV}}, \tag{3}$$

and $Q_\alpha > 1$ corresponds to a burning plasma. If the alpha particles deposit most of their energy inside the hotspot[9], then E_α can be readily obtained from the neutron measurements as

$$E_\alpha = 3.5\,\text{MeV} \times \int_0^{t_{bang}} \dot{n}_{DT}(t)\mathrm{d}t \approx 3.5\,\text{MeV} \times \frac{1}{2} Y_{DT}, \tag{4}$$

where $\dot{n}_{DT}$ is the DT fusion reaction rate, t_{bang} is the time of peak neutron production and Y_{DT} is the total yield from DT fusion reactions. In the presence of large spatial asymmetries and/or small hotspot areal densities (>0.2 g cm^{-2}), a large fraction of the alpha particles do not slow down inside the hotspot and E_α needs to account for the absorbed fraction θ_α of alpha particles. Both θ_α and E_{PdV} cannot be measured directly from experiments and therefore, a number of alternative metrics have also been devised as proxies for Q_α via a combination of analytic theory and simulations. The metrics considered here are summarized in Table 1 and include burning-plasma threshold parameters derived by Hurricane et al.[12,26,27], Christopherson et al.[8] and Betti et al.[9]. The metrics in Table 1 are then assessed via a Betti–Williams (BW) quasi-analytic, non-isobaric two-temperature model that is described in ref. 25, as well as one-dimensional (1D) simulations[28] that are tightly constrained by a comprehensive suite of diagnostic measurements. The Betti and Christopherson χ_α metrics were designed to remain valid even in the presence of large asymmetries; nevertheless, two-dimensional (2D) simulations[29] are used to verify this. Details on the reconstruction process can be found in the Methods.

Figure 1 shows how implosions on OMEGA have increased performance from the best performers in ref. 18 (orange circles) by increasing the energy coupling and transfer to the hotspot. The ultra-high velocity (~600 km s^{-1}) liner implosions[25,30] (magenta diamonds) focused on optimizing the fusion yield by maximizing the energy transferred to the hotspot at the cost of convergence, reaching the highest fusion yield recorded on OMEGA. However, since these implosions have reduced convergence, they do not reach the highest pressures and do not achieve a burning plasma when scaled hydro-equivalently in size by ×4.2. The 'χ-Optimization' (blue squares) instead focused on optimizing $\chi_{no\alpha}$ by increasing the energy coupling while maintaining a high target convergence and areal density, thereby maximizing $\chi_{no\alpha}$ and hotspot pressure to 0.195 ± 0.005 and 78 ± 7 Gbar, respectively, on OMEGA (Fig. 1b), which are their highest values to date. A schematic of the initial conditions of one of these implosions, shot 104949, is shown in Fig. 2.

Table 1 | The burning-plasma metrics considered in this work

Metric	Condition
Q_α	$Q_\alpha > 1$
Christopherson χ_α	$\chi_\alpha > 1.1$
Christopherson F_α	$F_\alpha > 0.7$
Betti $\chi_{no\alpha}$	$\chi_{no\alpha} > 0.8$
Betti $\hat{Y}$	$\hat{Y} = Y_\alpha / Y_{no\alpha} > 3.5$
Hurricane H_α	$H_\alpha = 5.3 \times 10^{25} \rho R_{hs} \frac{\langle \sigma v \rangle}{T_i v_{imp}} > 1$

$Q_\alpha > 1$ and Christopherson's metrics follow the methodology in ref. 8. Betti's metrics can be found in ref. 9. The modified Hurricane metric is described in ref. 12. These metrics are assessed where applicable using 1D analytic models and 1D and 2D simulations constrained by the suite of OMEGA diagnostics and hydro-equivalently scaled to 2.15 MJ of incident laser energy. Q_α is the definition of the burning-plasma parameter from equation (3). F_α is the ratio of alpha-heating work to hotspot internal energy. χ_α and $\chi_{no\alpha}$ are the normalized Lawson parameter from equation (1) evaluated with and without alpha heating, respectively. $\hat{Y}$ is the yield amplification due to alpha heating from equation (2). ρR_{hs} is the hotspot areal density, $\langle \sigma v \rangle$ is the Maxwellian-averaged reactivity for the DT fusion reaction, T_i is the average ion temperature and v_{imp} is the maximum velocity of the imploding shell.

Hydro-equivalent scaling with the BW model

Scaling these higher convergence implosions hydro-equivalently to 2.15 MJ of incident driver energy using the BW model gives $\chi_{no\alpha} \approx 0.86 \pm 0.02$ for the improved implosions (Fig. 1c), satisfying the Betti $\chi_{no\alpha}$ criterion for burning plasmas. By construction, the Betti $\hat{Y}$ criterion is also satisfied. The BW model cannot self-consistently account for alpha-heating effects, since it is scaled from implosions lacking alpha heating; consequently, only the Betti $\chi_{no\alpha}$ and $\hat{Y}$ criteria can be inferred using the BW model.

Hydro-equivalent scaling using LILAC and DRACO simulations

For a more sophisticated and self-consistent analysis, we turn to 1D LILAC[28] and 2D DRACO[29] simulations. We show in Table 2 results for one of the six experiments that exceed the Betti $\chi_{no\alpha}$ metric for burning plasmas in Fig. 1c, shot 104949. The other experiments have similar designs and results and the conclusions reached via this analysis will apply to them as well. The 1D simulations are degraded by reducing energy coupling and increasing coasting to reproduce the ion temperature T_i, electron temperature T_e, neutron yield Y_{DT}, areal density ρR, burn width τ, hotspot size R_{17} and time of peak neutron production t_{bang} measured in experiments (Table 2). The 2D simulations are instead degraded by adding 2D asymmetry sources until the yield matches experiments ($Y_{2D}/Y_{1D} \approx 0.2$–$0.4$). Details on the reconstruction process can be found in the Methods.

The simulations are then hydro-equivalently scaled up in laser energy with and without alpha heating to assess the metrics in Table 1 as a function of $\chi_{no\alpha}$. Figure 3 verifies that when the hotspot is ×4.2 larger (corresponding to a hydro-scaled incident driver energy of 2.15 MJ), the best-performing OMEGA implosions which have $\chi_{no\alpha} = 0.86 \pm 0.02$ pass all the burning-plasma threshold metrics in Table 1, with the 2D simulation results verifying that the relationship between $\chi_{no\alpha}$ and the other burning-plasma metrics in Table 1 remains valid even in the presence of strong perturbations.

To assess the extrapolated fusion yield, we first use the LILAC simulations to assess the yield amplification due to alpha heating $\hat{Y} = 5.8 \pm 0.7$ at $\chi_{no\alpha} = 0.86 \pm 0.02$. We use LILAC to assess $\hat{Y}(\chi_{no\alpha})$ rather than the analytic relation from ref. 9, as that relation has a

https://doi.org/10.1038/s41567-023-02361-4

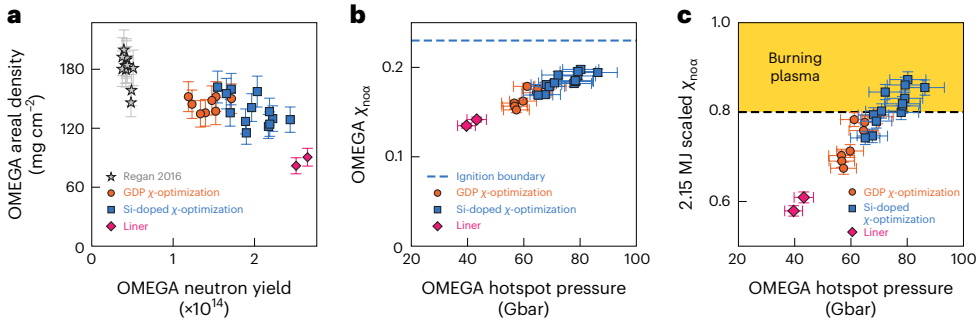

Fig. 1 | Experimental and 1D model burning-plasma metrics. a, Average measured neutron yields and areal densities for selected* OMEGA high-performance experiments. **b**, OMEGA pressures and generalized Lawson parameter $\chi_{noα}$ for selected* OMEGA high-performance experiments, **c**, Pressures and $\chi_{noα}$ for relevant OMEGA high-performance experiments hydro-equivalently scaled to 2.15 MJ of incident driver energy. Grey stars are the experiments from ref. 20 and orange circles from ref. 18. Magenta diamonds are the ultra-high (>600 km s^{-1}) liner implosions described in refs. 25,30 that were designed to maximize fusion yield, while the blue squares are the enhanced designs presented in this work designed to optimize $\chi_{noα}$. Orange-shaded regions in **c** correspond to a burning plasma according to the Betti $\chi_{noα}$ metric. The dashed line in **b** corresponds to the ignition boundary when OMEGA experiments are hydro-equivalently scaled to 2.15 MJ of incident driver energy. The dashed line in **c** corresponds to the burning-plasma onset boundary. Inferred values come from the BW model described in ref. 25 and the Methods. Error bars are one-standard-deviation ranges representing in **a**, the precision and in **b** and **c**, the precision of the measurements propagated through the model. The enhanced designs presented in this work achieved higher neutron yields while maintaining areal densities by increasing laser coupling efficiency. This has increased both pressure and $\chi_{noα}$ to the highest values achieved on OMEGA. The BW model in **c** suggests that six high-performance implosions now scale to a burning plasma after improvements in performance from ref. 18. In **a** and **b**, only a limited number of high-performance OMEGA experiments are shown, to preserve the clarity of the presentation.

singularity as $\chi_{noα} \to 1$ and is therefore not expected to be accurate as $\chi_{noα} \to 1$. Using hydro-equivalent scaling theory (Extended Data Table 1), the no-alpha yield of the experiments with a ×4.2 larger core is estimated as $Y_{DT}^{noα} = (9.7 \pm 1.0) \times 10^{16}$ neutrons, and the extrapolated fusion yield is then calculated as $\hat{Y} \times Y_{DT}^{noα} = 1.6 \pm 0.3$ MJ at a hydro-scaled incident driver energy of 2.15 MJ. This represents an approximately ×2 increase over the implosions of ref. 18 extrapolated with the same increase in core size (Fig. 4). While this is short of expecting a net energy gain from fusion, it is important to note that due to the proximity of the scaled implosions to the ignition cliff, even slight improvements in OMEGA performance will result in substantial increases in expected fusion energy, with gain expected when $\chi_{noα} > 0.9$.

Design of the highest performance LDD experiments

In this section, we describe the design modifications that led to the substantial performance improvements described above. The performance of an LDD implosion is a strong function of the energy coupled to the payload[31]. Absorption of the laser driver in LDD experiments is substantially degraded by cross-beam energy transfer (CBET)[32], which diverts energy away from the incoming laser beam into the outgoing rays. For LDD, the outgoing rays that primarily divert energy through CBET are those that refract around the target. In ref. 18, CBET was mitigated by steadily increasing the initial size of the target relative to the beams thus reducing the rays missing the target, though they still have a substantial reduction in laser absorption due to CBET (in the range ~75–95%). As explained in refs. 22,23, however, the size of the target cannot be increased indefinitely, as the overlapped beams apply their illumination asymmetry onto the target and eventually drive perturbations that compromise it.

To continue increasing absorption while mitigating CBET, we increased the atomic number Z of the coronal plasma by addition of a silicon dopant to the ablator, enhancing collisional absorption. This reduces the intensity of the pump rays and simultaneously increases the temperature of the coronal plasma, both of which reduce the CBET loss rate and increase absorption. Controlled experiments verified these effects and found that the addition of Si dopant to the ablator increased absorbed energy by ~10% for the designs of ref. 18. However, the higher Z of the coronal plasma also reduces conduction efficiency

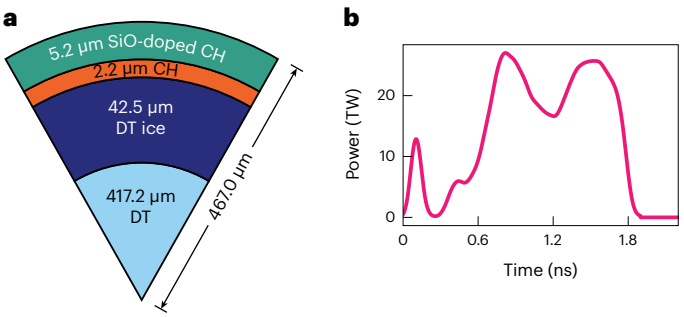

Fig. 2 | Initial conditions for the best-performing OMEGA shot 104949. **a**, A diagram of the target, with a large DT gas void in the centre, a DT ice layer, an inner carbon–deuterium polymer ablator and an outer carbon–hydrogen (CH) polymer ablator doped with silicon. **b**, The laser power history profile.

as noted in ref. 32, increases the initial mass of the target and increases radiative preheat of the payload. Partial mitigation of CBET also allows access to higher drive intensities and increases hydrodynamic efficiency, but at the cost of increasing the vulnerability to perturbation growth due to the higher acceleration and in-flight aspect ratio (IFAR). Higher intensities are also expected to amplify the two-plasmon decay[33] (TPD) and stimulated Raman scattering[34] (SRS) instability, but the higher coronal temperature from enhanced absorption was expected to offset this[33].

Finding the optimal tradeoff between these factors with a limited number of experiments requires accurate predictive capabilities, which are provided by the approach from ref. 18. The Z of the corona is increased by adding 5–7% atomic fraction Si dopant to the ablator, and an additional layer of undoped plastic is inserted between the doped ablator and payload to reduce the effect of radiative preheat and conduction efficiency loss. The resulting changes in the design can be seen in Extended Data Fig. 3. As CBET mitigation is stronger, higher laser intensities can be coupled efficiently to the target. This leads to a higher drive pressure, which would increase the IFAR and increase vulnerability to perturbation growth. In response, the total mass was increased, keeping the IFAR constant. The laser pulse is modified in a manner that keeps the coast time minimized, that is, the time between

https://doi.org/10.1038/s41567-023-02361-4

Table 2 | Experimental and degraded LILAC results for OMEGA shot 104949

Source	Y_{DT} (10^{14})	T_i (keV)	T_e (keV)	ρR (mg cm^{-2})	τ (ps)	R_{17} (μm)	t_{bang} (ps)	P_{hs} (Gbar)	$\chi_{noα}$
Shot 104949	(2.1±0.02)	4.6±0.3	3.8±0.1	160±15	70±5	27±0.1	2,000±50	78±7	0.195±0.005
LILAC	2.3	4.6	3.6	150	72	27	2000	75	0.20

The 1D LILAC simulations are degraded to broadly match the observed core conditions. Error ranges represent one standard deviation. The simulations closely match the experimental results, with simulated pressures and normalized Lawson parameter $\chi_{noα}$ within the inference uncertainty. T_i is the average ion temperature, T_e is the average electron temperature, τ is the time over which neutrons are produced, R_{17} is the average radius of the 17% contour in X-ray images of the hotspot, t_{bang} is the time of peak neutron production, P_{hs} is the average hotspot pressure.

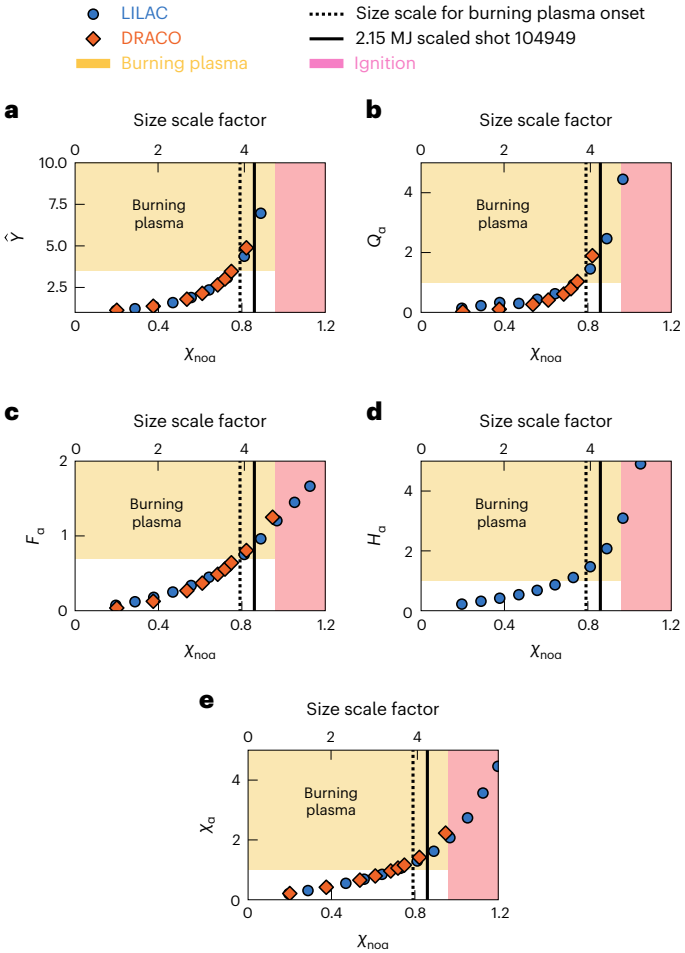

Fig. 3 | burning-plasma metrics for hydro-equivalent reconstructions of implosion in shot 104949. a, Betti $\hat{Y}$, the amplification of yield due to alpha heating[9]. **b**, $Q_α$, the definition of a burning plasma[8]. **c**, Christopherson $F_α$, the ratio of the alpha-heating work to the hotspot internal energy[8]. **d**,**e**, Hurricane $H_α$ (**d**) (ref. 12) and Christopherson $\chi_α$ (**e**), the normalized Lawson criterion evaluated in the presence of alpha heating[8] from Table 1 are shown versus the Betti $\chi_{noα}$ metric[9] (lower axis) and size scaling factor (upper axis) for hydro-equivalently scaled 1D LILAC (blue circles) and 2D DRACO (magenta squares) simulations. The orange-shaded region corresponds to a burning plasma for the displayed metric, while the red-shaded region corresponds to ignition according to $\chi_{noα} \approx 1$. The solid black line indicates the value of $\chi_{noα} = 0.86 \pm 0.02$ for the best-performing implosion (shot 104949) scaled up hydro-equivalently by ×4.2 in size, corresponding to 2.15 MJ of driver energy. $\hat{Y}$ The dotted vertical black line shows the minimum size scale of ×3.9 at which the OMEGA experiments extrapolate to a burning plasma according to the Betti $\chi_{noα}$ metric. The LILAC simulations are degraded to closely match shot 104949, while the DRACO simulations are degraded with 2D asymmetries to have a similar yield degradation ($Y_{2D}/Y_{1D} \approx 0.2$–$0.4$) as in the experiments. A burning plasma is expected within uncertainty for the scaled conditions of shot 104949 according to all the burning-plasma metrics, even if the hotspot were highly perturbed. At large values of $\chi_{noα}$, the 2D alpha-on metrics are higher than expected as alpha heating reduces the growth rate of instabilities[6].

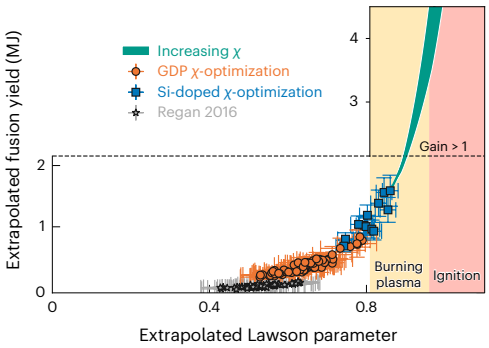

Fig. 4 | Progress toward hydro-equivalent ignition. We show the corresponding increase in the extrapolated fusion energy at 2.15 MJ of incident laser energy for cryogenic direct-drive implosions on OMEGA from 2015 to present and expected trajectory for future experiments, pending affirming trials. Progress toward hydro-equivalent ignition is measured by the extrapolated Lawson parameter $\chi_{noα}$ from equation (1) inferred using the Betti–Williams model and extrapolated using the hydro-equivalent scaling relations of refs. 16–18. Orange circles and grey stars are the implosion series that culminated in those of ref. 18 and ref. 20, respectively, while blue squares are the implosions described in this work. The black dashed line shows the gain = 1 boundary, above which the extrapolated fusion energy exceeds 2.15 MJ (black dashed line), and the implosion produces net energy. Error bars show the one-standard-deviation range for the experimentally measured uncertainties propagated through the Betti–Williams model by Monte Carlo estimation. The orange-shaded region corresponds to a burning plasma, while the red-shaded region corresponds to ignition according to refs. 8,9. The green region is the path that future implosions are expected to follow if they are successful in increasing $\chi_{noα}$, with the upper and lower bounds given by implosions that improve $\chi_{noα}$ only by increasing the yield and areal density, respectively. If $\chi_{noα}$ can be increased by ~5% to above 0.9, implosions are expected to extrapolate to gain greater than unity, and if $\chi_{noα}$ can be increased by ~10% to above 0.96, ignition and several megajoule yields are expected.

the end of the laser driven acceleration and when the shell begins to decelerate[35,36]. Despite the increase in mass, the final implosion velocity of the Si-doped targets remains higher than the original design, leading to a substantial increase in yield (~30%). The various modifications to the design are guided by the Statistical Model to keep constant the yield degradation with respect to LILAC, allowing the gains made in simulations to be reflected in experiments. The increased coronal temperature also reduced the TPD threshold proximity parameter, which reduced hot-electron preheat and allowed the areal density to remain constant in experiments despite the increase in radiative preheat.

The next step for the LDD programme on OMEGA is to achieve hydro-equivalent gain and ignition. This will require increasing the extrapolated $\chi_{noα}$ 10% above current levels. As $\chi_{noα} \to 0.96$, the yield amplification will sharply increase (Fig. 3a), and the extrapolated implosions will likely reach an extrapolated gain greater than 1 before extrapolated ignition occurs (Fig. 4). Confidence in the hydro-equivalent result will require more robust verification of the scaling behaviour of implosion experiments between OMEGA and the NIF. A series of direct-drive experimental campaigns are currently underway[33,37,38]

to characterize laser-plasma instabilities, energy coupling and hot-electron preheat at megajoule scale on the NIF to better understand scaling and to quantify deviations from hydro-equivalency. The most recent results[38] from this effort in point toward only minor deviations from hydro-equivalence. Achieving hydro-equivalent ignition and expectations of multi-megajoule yields based on OMEGA experiments will require some combination of an increase of 50% in the OMEGA fusion yield and an increase of 20% in the OMEGA areal density. Upcoming experiments on OMEGA will attempt to achieve this by subcooling the cryogenic layer to increase convergence independently of target entropy and by using the small-spot SG5-650 phase plates[39] to increase laser intensity and ablation pressure above what is presently used for high-performance OMEGA implosions. However, even if hydro-equivalent ignition is achieved on OMEGA, the current high performing designs will have an extrapolated gain less than 10. Achieving higher gains in conventional LDD would be aided by mitigation of laser-plasma instabilities to increase ablation pressure and reduction of the high mode imprint of the laser beams to stabilize high convergence implosions. Advanced target designs[40,41] and high bandwidth solid-state[42] or excimer[43] laser systems provide a path toward mitigation of CBET[44], TPD and SRS[45], and laser imprint[40–42], and these designs and systems are under active investigation.

Online content

Any methods, additional references, Nature Portfolio reporting summaries, source data, extended data, supplementary information, acknowledgements, peer review information; details of author contributions and competing interests; and statements of data and code availability are available at https://doi.org/10.1038/s41567-023-02361-4.

References

1. Nuckolls, J., Wood, L., Thiessen, A. & Zimmerman, G. Laser compression of matter to super-high densities: thermonuclear (CTR) applications. *Nature* **239**, 139–142 (1972).
2. Atzeni, S. & Meyer-ter-Vehn, J.*The Physics of Inertial Fusion: Beam Plasma Interaction, Hydrodynamics, Hot Dense Matter* 1st edn (Oxford Univ. Press, 2004); https://doi.org/10.1093/acprof:oso/9780198562641.001.0001
3. Lindl, J. D. *Inertial Confinement Fusion: The Quest for Ignition and Energy Gain Using Indirect Drive* (Springer-Verlag, 1998).
4. Craxton, R. S. et al. Direct-drive inertial confinement fusion: a review. *Phys. Plasmas* **22**, 110501 (2015).
5. Slutz, S. A. et al. Pulsed-power-driven cylindrical liner implosions of laser preheated fuel magnetized with an axial field. *Phys. Plasmas* **17**, 056303 (2010).
6. Chang, P. et al. Generalized measurable ignition criterion for inertial confinement fusion. *Phys. Rev. Lett.* **104**, 135002 (2010).
7. Spears, B. K. et al. Performance metrics for inertial confinement fusion implosions: aspects of the technical framework for measuring progress in the National Ignition Campaign. *Phys. Plasmas* **19**, 056316 (2012).
8. Christopherson, A. R. et al. Theory of ignition and burn propagation in inertial fusion implosions. *Phys. Plasmas* **27**, 052708 (2020).
9. Betti, R. et al. Alpha heating and burning plasmas in inertial confinement fusion. *Phys. Rev. Lett.* **114**, 255003 (2015).
10. Betti, R. & Hurricane, O. A. Inertial-confinement fusion with lasers. *Nat. Phys.* **12**, 435–448 (2016).
11. Hurricane, O. A. et al. Inertially confined fusion plasmas dominated by alpha-particle self-heating. *Nat. Phys.* **12**, 800–806 (2016).
12. Zylstra, A. B. et al. Burning plasma achieved in inertial fusion. *Nature* **601**, 542–548 (2022).
13. Kritcher, A. L. et al. Design of inertial fusion implosions reaching the burning plasma regime. *Nat. Phys.* **18**, 251–258 (2022).
14. Abu-Shawareb, H. et al. Lawson Criterion for ignition exceeded in an inertial fusion experiment. *Phys. Rev. Lett.* **129**, 075001 (2022).
15. Hawker, N. A simplified economic model for inertial fusion. *Philos. Trans. R. Soc. A* **378**, 20200053 (2020).
16. Nora, R. et al. Theory of hydro-equivalent ignition for inertial fusion and its applications to OMEGA and the National Ignition Facility.*Phys. Plasmas* **21**, 056316 (2014).
17. Bose, A. et al. Core conditions for alpha heating attained in direct-drive inertial confinement fusion. *Phys. Rev. E* **94**, 011201 (2016).
18. Gopalaswamy, V. et al. Tripled yield in direct-drive laser fusion through statistical modelling. *Nature* **565**, 581–586 (2019).
19. Ding, Y. H., White, A. J., Hu, S. X., Certik, O. & Collins, L. A. Ab initio studies on the stopping power of warm dense matter with time-dependent orbital-free density functional theory. *Phys. Rev. Lett.* **121**, 145001 (2018).
20. Regan, S. P. et al. Demonstration of fuel hot-spot pressure in excess of 50 Gbar for direct-drive, layered deuterium-tritium implosions on OMEGA. *Phys. Rev. Lett.* **117**, 025001 (2016).
21. Mannion, O. M. et al. Mitigation of mode-one asymmetry in laser-direct-drive inertial confinement fusion implosions. *Phys. Plasmas* **28**, 042701 (2021).
22. Lees, A. et al. Experimentally inferred fusion yield dependencies of OMEGA inertial confinement fusion implosions. *Phys. Rev. Lett.* **127**, 105001 (2021).
23. Gopalaswamy, V. et al. Using statistical modeling to predict and understand fusion experiments. *Phys. Plasmas* **28**, 122705 (2021).
24. Lees, A. et al. Understanding the fusion yield dependencies in OMEGA DT-layered implosion experiments using a physics-based statistical mapping model. *Phys. Plasmas* **30**, 012709 (2023).
25. Williams, C. et al. First demonstration of hot-spot fuel gain exceeding unity in cryogenic direct-drive inertial confinement fusion. *Nat. Phys.* https://doi.org/10.1038/s41567-023-02363-2 (2024).
26. Hurricane, O. A. et al. Beyond alpha-heating: driving inertially confined fusion implosions toward a burning-plasma state on the National Ignition Facility. *Plasma Phys. Contr. F.* **61**, 014033 (2018).
27. Hurricane, O. A. et al. Approaching a burning plasma on the NIF. *Phys. Plasmas* **26**, 052704 (2019).
28. Delettrez, J., Epstein, R., Richardson, M. C., Jaanimagi, P. A. & Henke, B. L. Effect of laser illumination nonuniformity on the analysis of time-resolved X-ray measurements in uv spherical transport experiments. *Phys. Rev. A* **36**, 3926–3934 (1987).
29. Radha, P. B. et al. Two-dimensional simulations of plastic-shell, direct-drive implosions on OMEGA. *Phys. Plasmas* **12**, 032702 (2005).
30. Williams, C. A., Betti, R., Gopalaswamy, V. & Lees, A. High yields in direct-drive inertial confinement fusion using thin-ice DT liner targets. *Phys. Plasmas* **28**, 122708 (2021).
31. Zhou, C. D. & Betti, R. Hydrodynamic relations for direct-drive fast-ignition and conventional inertial confinement fusion implosions. *Phys. Plasmas* **14**, 072703 (2007).
32. Igumenshchev, I. V. et al. Crossed-beam energy transfer in implosion experiments on OMEGA. *Phys. Plasmas* **17**, 122708 (2010).
33. Solodov, A. A. et al. Hot-electron preheat and mitigation in polar-direct-drive experiments at the National Ignition Facility. *Phys. Rev. E* **106**, 055204 (2022).
34. Rosenberg, M. J. et al. Origins and scaling of hot-electron preheat in ignition-scale direct-drive inertial confinement fusion experiments. *Phys. Rev. Lett.* **120**, 055001 (2018).

35. Lindl, J., Landen, O., Edwards, J. & Moses, E., NIC Team. Review of the National Ignition Campaign 2009-2012. *Phys. Plasmas* **21**, 020501 (2014).
36. Hurricane, O. A. et al. On the importance of minimizing 'coast-time' in X-ray driven inertially confined fusion implosions. *Phys. Plasmas* **24**, 092706 (2017).
37. Marozas, J. A. et al. First observation of cross-beam energy transfer mitigation for direct-drive inertial confinement fusion implosions using wavelength detuning at the National Ignition Facility. *Phys.Rev. Lett.* **120**, 085001 (2018).
38. Rosenberg, M. J. et al. Hot electron preheat in hydrodynamically scaled direct-drive inertial confinement fusion implosions on the NIF and OMEGA. *Phys. Plasmas* **30**, 072710 (2023).
39. Theobald, W. et al. Enhanced laser-energy coupling with small-spot distributed phase plates (SG5-650) in OMEGA DT cryogenic target implosions. *Phys. Plasmas* **29**, 012705 (2022).
40. Hu, S. X. et al. Mitigating laser-imprint effects in direct-drive inertial confinement fusion implosions with an above-critical-density foam layer. *Phys. Plasmas* **25**, 082710 (2018).
41. Ceurvorst, L. et al. Hybrid target design for imprint mitigation in direct-drive inertial confinement fusion. *Phys. Rev. E* **101**, 063207 (2020).
42. Dorrer, C., Hill, E. M. & Zuegel, J. D. High-energy parametric amplification of spectrally incoherent broadband pulses. *Opt. Express* **28**, 451–471 (2020).
43. Obenschain, S. et al. High-energy krypton fluoride lasers for inertial fusion. *Appl. Optics* **54**, F103–F122 (2015).
44. Bates, J. W. et al. Suppressing cross-beam energy transfer with broadband lasers. *High Energy Density Phys.* **36**, 100772 (2020).
45. Follett, R. K. et al. Thresholds of absolute two-plasmon-decay and stimulated Raman scattering instabilities driven by multiple broadband lasers. *Phys. Plasmas* **28**, 032103 (2021).

Methods

Hydro-equivalent scaling

The 2.15 MJ NIF is currently the sole facility in the world with the capability to implode targets which can achieve significant alpha heating. However, the laser configuration and target delivery systems presently available on the NIF make it incapable of carrying out symmetric LDD experiments. Instead, these experiments are performed at the 30 kJ OMEGA Laser Facility, which is the leading symmetric LDD experimental facility in the world. As the OMEGA laser has ~70 times less energy, implosions on OMEGA cannot achieve conditions in which significant alpha heating will occur, since the size of the fusion plasma R_{hs} is much smaller than the alpha-particle mean-free-path λ_α. Therefore, we assess progress in LDD by scaling the observed implosions on OMEGA up in size, keeping intrinsic quantities such as hotspot pressure P_{hs}, implosion velocity or fuel entropy constant so that the increase in alpha heating at larger scales is only due to the increase in size leading to $R_{hs} > \lambda_\alpha$ and not in implosion quality. This is an established method known as hydro-equivalent scaling[16–18].

The increase in size can be connected to a required driver energy (E_{driver}), using the transfer efficiency η and hotspot energy E_{hs}, where

$$E_{hs} \propto R_{hs}^3 P_{hs} \propto \eta(E_{driver}) E_{driver}, \tag{5}$$

so the energy required to produce a hotspot with radius R_{hs} at a fixed pressure P_{hs} scales like

$$E_{driver} \propto \frac{R_{hs}^3}{\eta(E_{driver})}. \tag{6}$$

In hydro-equivalent scaling, we assume $\eta(E_{driver}) \equiv \eta$ does not vary with E_{driver}, so that the required driver energy scales like

$$E_{driver} \propto R_{hs}^3. \tag{7}$$

For a given implosion design, there are a variety of 1D physics effects which could affect the scaling of η with E_{driver} either negatively (for example CBET, TPD and SRS) or positively (collisional absorption[4], Knudsen-layer reactivity reduction[46] or barodiffusion[47]). There are also a number of three-dimensional perturbation sources that affect η which are unique to OMEGA and are not intrinsic to LDD such as the restriction of ablator material to those which are amenable to diffusion filling, the damage inflicted on the ablator due to the diffusion filling process, the large (~15 μm) mounting stalk, the 60-beam spherical geometry or the laser speckle pattern. Many of these engineering features are different on the NIF—for instance, the NIF uses a fill-tube filling process, which does not damage the ablator and allows for advanced ablator materials such as beryllium or high-density carbon, but also has 192 beams arranged in a polar configuration.

Given the large range of possibilities, we choose to forego making any assumptions—positive or negative—on the scaling of η in favour of keeping it constant. Consequently, the results presented in this work are a statement about the quality of the implosions achieved on OMEGA, by assessing the performance of these implosions if the stagnated configurations were reproduced with identical quality at larger energy scales that are achievable at present. During the process of hydro-equivalent scaling to larger sizes by a factor S, we require only that

- The pressure P_{hs} of OMEGA implosions remains constant with S
- The hotspot energy E_{hs} increases as S^3
- The hotspot energy $E_{hs} \propto S^3$ of OMEGA implosions increases as the driver energy E_{driver} (that is, there is no change in transfer efficiency), so that $E_{driver} \propto S^3$

In refs. 16,17, hydro-equivalent scaling theory is used to derive the relationship between size or energy and the yield ($Y_{noα}$), areal density ($\rho R_{noα}$) and $\chi_{noα}$. The scaling relations are all parametrized as

$$X\text{scaled} = X_{OMEGA} \times \left(\frac{E_{scaled}}{E_{OMEGA}}\right)^{\beta}, \tag{8}$$

$$= X_{OMEGA} \times \left(\frac{R_{scaled}}{R_{OMEGA}}\right)^{3\beta}, \tag{9}$$

where X is the observable of interest, E and R represent the energy or size at which the observable is measured at OMEGA or inferred at some scaled energy, and β is the energy scale exponent for the observable. A list of the relevant β inferred by ref. 17 are reproduced in Extended Data Table 1.

To be certain that the results from refs. 17,48 are applicable to the implosion dynamics in this work, we also hydro-equivalently scaled the 1D LILAC and 2D DRACO reconstructions of shot 104949. To scale implosion simulations, we first run them at the OMEGA scale up to the point where the laser drive ends. The simulation is then increased in size in a hydro-equivalent manner and continued at a variety of scales with and without alpha-particle transport. Extended Data Fig. 2 shows that the simulations act as expected in the absence of alpha heating, following existing hydro-equivalent scaling theory in ref. 17. A list of the relevant β inferred from the hydro-equivalently scaled LILAC simulations is also reported in Extended Data Table 1.

To explore the validity of hydro-equivalent scaling theory in experiments, there is a large, active research collaboration[33,34,37,38] exploring laser-plasma interaction physics and how they vary between OMEGA and NIF. In recent investigations into the scaling of hot-electron preheat, Rosenberg et al.[38] compared implosion experiments on OMEGA and NIF, which were both driven with minimal beam smoothing[49] and in a polar configuration[50] These experiments increased energy from ~17 kJ on OMEGA to ~700 kJ on NIF by roughly 40 times, corresponding to an increase in S to ~3.5. They show that the integrated effect of SRS at the NIF scale is similar to the integrated effect of TPD at the OMEGA scale (SRS is the dominant mechanism at NIF and TPD at OMEGA), verifying that hot-electron preheat (that is energy deposited into the shell per unit mass) scales hydro-equivalently between OMEGA and NIF. Rosenberg et al. also show measured in-flight trajectories from the X-ray self-emission images of OMEGA and NIF implosions and find that the implosion velocities are similar, with NIF implosions being slightly slower than OMEGA. The nuclear yield measurements from these implosions can also be used to calculate an experimental value for β to compare to the hydro-equivalent theory. These data are reported in Extended Data Fig. 1 and Extended Data Table 1 and suggest that the yield increase as implosions are scaled up in energy from OMEGA to NIF is consistent with hydro-equivalent scaling theory. Nevertheless, many open questions remain on the details of scaling physics between OMEGA and NIF energies, and there is not yet a clear path to fielding high-performance cryogenic implosions on the NIF due to the many differences in the target delivery and laser beam properties between NIF and OMEGA. However, these results provide experimental support for hydro-equivalent scaling as a reasonable extrapolation method from OMEGA to NIF energies.

Core reconstruction

OMEGA diagnostics. The stagnated core reconstruction process is tightly constrained by a comprehensive suite of diagnostics available on OMEGA. Neutron yields, fusion plasma ion temperatures and fluid velocities[51] are measured via a suite of neutron-time-of-flight (nTOF) detectors placed around the OMEGA target chamber that measure DT and deuterium–deuterium (DD) fusion reactions. Areal densities are measured by nTOF backscatter[52] and a magnetic recoil spectrometer[53] (MRS) forward scatter diagnostic. Hotspot X-ray images[54,55] are

measured from the GMXI[56], TRXI[54], KB-FRAMED[57] and SRTe[55] diagnostics, which view the core from various lines of sight. The fusion burn duration and time of peak burn are measured by the Neutron Temporal Diagnostic. Finally, the electron temperature is measured by the SRTe diagnostic[55]. Owing to excellent symmetry control on OMEGA[21], the best-performing implosions considered in this work show only marginal asymmetry signatures, with low variation in the apparent ion temperatures measured from the width of the 14.03 MeV neutron spectrum[23,58] ($T_{i,max}/T_{i,min} = 1.08 \pm 0.1$) and areal densities ($\rho R_{max}/\rho R_{min} = 1.0 \pm 0.1$) and low bulk flow velocities ($v_{fluid}/v_{shell} = 0.1 \pm 0.1$), as well as nearly circular X-ray images (ellipse major–minor axis ratio ~1.1 ± 0.1).

The quasi-analytic Betti–Williams model. Calculating $\chi_{n\alpha}$ from equation (1) requires knowledge of the mass of the deuterium–tritium portion of the confining shell affected by the return shock. This quantity cannot be measured in an implosion and must instead be inferred from other experimental measurements. This inference can be carried out using simulations or analytic models constrained by experiments. The companion paper ref. 25 describes a quasi-analytic, non-isobaric, two-temperature, static Betti–Williams model; we provide a short description here, as well. This is similar to the approach used in ref. 12, though the details differ due to the differences in diagnostic capabilities between the NIF and OMEGA. Uncertainties in the model-estimated parameters are obtained by Monte Carlo estimation, assuming the uncertainties in the experimental inputs are normally distributed and independent. We begin by noting that the fusion yield is given by

$$Y_{DT} = \int n_D n_T \langle \sigma v \rangle \, \mathrm{d}V \mathrm{d}t, \tag{10}$$

where n_D, n_T and $\langle \sigma v \rangle$ are the deuterium and tritium number density and the Maxwell-averaged fusion reactivities of the DT fusion reaction, respectively. These are averaged over space and time to obtain the fusion yield. Assuming an ideal gas, equation (10) can be rewritten as

$$Y_{DT} = \int P_i^2 f_D f_T \frac{\langle \sigma v \rangle}{T_i^2} \, \mathrm{d}V \mathrm{d}t, \tag{11}$$

where f_D, f_T, P_i and T_i are the deuterium and tritium number fractions, ion pressure and temperature, respectively. We then assume that the time dependence can be eliminated by assuming that the bulk of the fusion reactions occur over a short time scale compared to the hydrodynamic time scale, so that

$$Y_{DT} = A\tau \int P_i^2 f_D f_T \frac{\langle \sigma v \rangle}{T_i^2} \, \mathrm{d}V, \tag{12}$$

where τ is the full-width at half-maximum of the neutron production history and A is a constant to be determined. The spatial dependence of equation (12) is handled by assuming spherical symmetry and writing each spatially varying quantity $q(r)$ as

$$q(r) = q_0 \hat{q}(r), \tag{13}$$

where $\hat{q}(r)$ is a non-dimensional shape function and q_0 is the value at $r = 0$ for the quantity q. Applying this to equation (12), we obtain

$$Y_{DT} = A\tau \frac{4\pi P_{i0}^2 \langle \sigma v \rangle_0}{T_{i0}^2} R_{hs}^3 I, \tag{14}$$

where I is a non-dimensional profile integral

$$I = \int_0^1 \hat{P}_i^2(\hat{r}) f_D(\hat{r}) f_T(\hat{r}) \frac{\langle \hat{\sigma v} \rangle(\hat{r})}{\hat{T}_i^2(\hat{r})} \hat{r}^2 \, \mathrm{d}\hat{r}. \tag{15}$$

For the electronic contribution to pressure and energy, we assume the hotspot consists of only a fully ionized DT plasma, so that

$$T_e(r) = T_i(r) \frac{\hat{P}_i}{\hat{P}_e} \frac{T_{i0}}{T_{e0}}. \tag{16}$$

If we did not make this correction and had assumed that $T_e = T_i$, on average this would increase pressures by 10–15%, since in reality $T_e < T_i \rightarrow P_e < P_i$, and since $P = P_e + P_i$, $P_{BW} < P_{equilibrated}$.

To solve this system, we need to specify the profile functions for electron and ion pressure and temperature. One choice for the profiles could be analytic, for example, the isobaric profiles from ref. 31. For improved accuracy, we use profiles from LILAC simulations of each implosion, instead of assuming that the pressure profile is flat (that is, isobaric). This is important because the Mach number of the hotspot (V_i/V_{sound}) » 0 and cannot be ignored for large ($V_i > 300$ km s^{-1}) implosion velocities. When the Mach number is large in the hotspot, the hotspot pressure decreases monotonically from its central value and is reduced by 20–40% at the hotspot–shell boundary.

The constant A can be determined by rewriting equation (12) as

$$Y_{DT} = A\tau \dot{Y}_{DT}, \tag{17}$$

where $\dot{Y}_{DT}$ is the peak neutron rate. The constant A then acts as a proportionality constant for the integral of the reaction rate over time—for instance, if the shape were purely Gaussian, $A = \sqrt{\pi/\ln(16)} \approx 1.06$. Since the reaction rate is actually slightly non-Gaussian, we find A from LILAC simulations to be ~1.1. Finally, the hotspot radius R_{hs} can be determined from any of several X-ray imaging diagnostics which integrate over different X-ray energy ranges. In an ideal scenario, R_{hs} would instead be measured from neutron images, as done at the NIF, but such a diagnostic is not presently available on OMEGA. Instead, to determine the optimal choice of X-ray energies we post-process LILAC simulations of all 350+ cryogenic implosions since 2014 with SPECT3D (ref. 59) to generate synthetic images of each real diagnostic and find that using the highest energy (~18–20 keV) X-ray image from the SRTe diagnostic provides self-consistent results when the Betti–Williams model is applied to these simulations. Using high photon energy X-ray images as a proxy for neutron images is supported by observations on the NIF and OMEGA[60] that the $E_\gamma \approx 15$–20 keV X-ray emission region is consistent with the spatial extent of the neutron emission. We choose the 17% contour of the images to remain consistent with previous work[8,20], as well as finding that it both encloses 93–95% of the neutron producing region in high implosion velocity LILAC simulations and has an acceptably low statistical uncertainty (~0.5 μm standard deviation) in experiments.

Once the hotspot has been reconstructed using the Betti–Williams model, the hotspot mass and areal density can be evaluated by integrating the hotspot density

$$\rho_{hs}(r) = \frac{P_i(r)}{T_i(r)}, \tag{18}$$

$$\rho R_{hs} = \int \rho_{hs}(r) \, \mathrm{d}r, \tag{19}$$

$$M_{hs} = \int \rho_{hs}(r) \, \mathrm{d}V, \tag{20}$$

and comparing to the measured areal density to obtain the shell areal density and mass

$$\rho R_{shell} = \rho R - \rho R_{hs}, \tag{21}$$

$$M_{shell} = 4\pi R_{hs}^2 \rho R_{shell} \left(1 + \frac{1}{A_{shell}} + \frac{1}{3A_{shell}^2}\right), \tag{22}$$

where A_{shell} is the stagnation (that is, at minimum radius) aspect ratio of the shell, estimated from LILAC so that the total mass is

$$M_{stag} = M_{hs} + M_{shell}. \quad (23)$$

We note that while the aspect-ratio correction used here requires an input from a simulation and cannot be corroborated with experimental evidence, it only acts to increase M_{stag} and reduce $\chi_{no\alpha}$ compared to the analysis in ref. 12, which is consistent with our analysis in the limit of infinite aspect ratio or an infinitesimally thin shell. LILAC stagnation aspect ratios are approximately 2 to 4, and we use an uncertainty of ±0.5 in the Monte Carlo propagation of uncertainties. This leads to an aspect-ratio correction factor that can increase M_{shell} by up to 60% for very low aspect ratio, thick shells.

Radiation-hydrodynamic simulations. 1D LILAC and 2D DRACO simulations are run using CBET, nonlocal thermal transport, multigroup radiation transport and first-principles equation-of-state tables, as well as multigroup alpha-particle transport for the alpha-on simulations. The as-shot pulse shape and target specifications are used to initialize the simulations. As the 1D LILAC simulations cannot have asymmetries introduced, it is degraded by reducing absorption until its bang-time matches experiment, after which point it is degraded by increasing the coasting time. The 2D DRACO simulations also have their absorption decreased until their bang-time matches experiments, but are then degraded by adding all known perturbation sources that can be modelled. This is insufficient to fully reconcile the observed yield degradation, so the laser imprint is artificially increased as a stand-in for the effects of defects in the ice and target until the yield degradation (Y_{2D}/Y_{1D}) matches the experiment (Y_{exp}/Y_{1D}). The simulations are postprocessed with SPECT3D and IRIS[61] to produce synthetic diagnostics which are compared to experiments.

The hotspot is defined as the region at the time of peak neutron production within the neutron R17 boundary, that is where neutron production

$$\dot{N} = n_D n_T \langle \sigma v \rangle \quad (24)$$

is greater than 17% of its peak value. In simulations, this choice of contour value is chosen to remain consistent with ref. 8. For times other than at peak neutron production, the fluid volume corresponding to this region is tracked backward or forward. This is trivial in LILAC, as it is a 1D Lagrangian code. In 2D DRACO simulations, the non-convex R17 boundary is reconstructed using an alpha-shape method and is tracked via advection of boundary tracer particles with a predictor-corrector method.

Data availability

Raw data were generated at the OMEGA Laser Facility. Derived data supporting the findings of this study are available from the corresponding author upon request and with permission from the OMEGA Laser Facility.

References

46. Molvig, K., Hoffman, N. M., Albright, B. J., Nelson, E. M. & Webster, R. B. Knudsen Layer reduction of fusion reactivity. *Phys. Rev. Lett.* **109**, 095001 (2012).
47. Amendt, P., Landen, O. L., Robey, H. F., Li, C. K. & Petrasso, R. D. Plasma barodiffusion in inertial-confinement-fusion implosions: application to observed yield anomalies in thermonuclear fuel mixtures. *Phys. Rev. Lett.* **105**, 115005 (2010).
48. Bose, A., Woo, K. M., Nora, R. & Betti, R. Hydrodynamic scaling of the deceleration-phase Rayleigh–Taylor instability. *Phys. Plasmas* **22**, 072702 (2015).
49. Boehly, T. R. et al. Optical and plasma smoothing of laser imprinting in targets driven by lasers with SSD bandwidths up to 1 THz. *Phys. Plasmas* **8**, 2331–2337 (2001).
50. Skupsky, S. et al. Polar direct drive on the National Ignition Facility. *Phys. Plasmas* **11**, 2763–2770 (2004).
51. Mannion, O. M. et al. A suite of neutron time-of-flight detectors to measure hot-spot motion in direct-drive inertial confinement fusion experiments on OMEGA. *Nucl. Instrum. Meth. A* **964**, 163774 (2020).
52. Forrest, C. J. et al. High-resolution spectroscopy used to measure inertial confinement fusion neutron spectra on Omega. *Rev. Sci. Instrum.* **83**, 10D919 (2012).
53. Gatu Johnson, M. et al. Measurement of apparent ion temperature using the magnetic recoil spectrometer at the OMEGA laser facility. *Rev. Sci. Instrum.* **89**, 101129 (2018).
54. Churnetski, K. et al. Three-dimensional hot-spot X-ray emission tomography from cryogenic deuterium-tritium direct-drive implosions on OMEGA. *Rev. Sci. Instrum.* **93**, 093530 (2022).
55. Shah, R. C. et al. Bound on hot-spot mix in high-velocity, high-adiabat direct-drive cryogenic implosions based on comparison of absolute X-ray and neutron yields. *Phys. Rev. E* **106**, L013201 (2022).
56. Oertel, J. A. et al. Framed monochromatic images of implosions taken with the joint LLE/LANL Gated Monochromatic X-ray Imager (GMXI). *Annual Meeting of the American Physical Society Division Of Plasma Physics* lWepP424 (American Physical Society, 1997).
57. Marshall, F. J. & Oertel, J. A. A framed monochromatic X-ray microscope for ICF (invited). *Rev. Sci. Instrum.* **68**, 735–739 (1997).
58. Munro, D. H. Interpreting inertial fusion neutron spectra. *Nucl. Fusion* **56**, 036001 (2016).
59. MacFarlane, J. J., Golovkin, I. E., Wang, P., Woodruff, P. R. & Pereyra, N. A. SPECT3D - A multi-dimensional collisional-radiative code for generating diagnostic signatures based on hydrodynamics and PIC simulation output. *High Energy Density Phys.* **3**, 181–190 (2007).
60. Cao, D. et al. Interpreting the electron temperature inferred from X-ray continuum emission for direct-drive inertial confinement fusion implosions on OMEGA. *Phys. Plasmas* **26**, 082709 (2019).
61. Gopalaswamy, V. et al. Analysis of limited coverage effects on areal density measurements in inertial confinement fusion implosions. *Phys. Plasmas* **29**, 072706 (2022).

Acknowledgements

We thank P. Patel for discussions on comparing neutron and X-ray imaging at the NIF. This material is based upon work supported by the Department of Energy National Nuclear Security Administration under Award Number DE-NA0003856, the Department of Energy Office of Fusion Energy Sciences under Award Numbers DE-SC0021072, DE-SC0022132 and DE-SC0024381, the University of Rochester and the New York State Energy Research and Development Authority. This report was prepared as an account of work sponsored by an agency of the US Government. Neither the US Government nor any agency thereof, nor any of their employees, makes any warranty, express or implied, or assumes any legal liability or responsibility for the accuracy, completeness, or usefulness of any information, apparatus, product, or process disclosed, or represents that its use would not infringe privately owned rights. Reference herein to any specific commercial product, process or service by trade name, trademark, manufacturer or otherwise does not necessarily constitute or imply its endorsement, recommendation or favouring by the US Government or any agency thereof. The views and opinions of authors expressed herein do not necessarily state or reflect those of the US Government or any agency thereof.

Author contributions

V.G. and R.B. conceived the study and wrote the paper. V.G., R.B., A.L. and R. Ejaz developed predictive models used to design

high-performance experiments. V.G., C.A.W., R.B., D.P., J.P.K., A.L., D.C., P.F., R. Epstein, C.A.T., W.T., M.J.R., S.P.R., C. Stoeckl, V.N.G. designed and executed experiments used in training the predictive models used for this work. V.G., C.A.W., R.B., D.P., J.P.K., A.L. designed and executed the high-performance experiment series. D.C., K.S.A., RE, J.C.-N., I.V.I., J.A.M., P.B.R., A.A.S., T.J.B.C., S.X.H., W.S. and V.N.G. contributed to the radiation-hydrodynamic simulation development used in this work. V.G., C.J.F., V.Y.G., W.T., D.H.E., S.I., M.J.R., H.M., M.G.-J., R.D.P., J.A.F. and S.P.R. contributed to development and analysis of diagnostics used in this work. D.B., C.F., M.K., R.T.J., M.J.B., J.M., B.S., D.G., C. Shulberg, M.F. and D.R.H. were responsible for fielding the implosion targets used in this work. K.A.B., S.S. and L.J.W. were responsible for managing the OMEGA laser. M.L. and S.F.B.M. were responsible for managing the OMEGA facility and experimental operations. E.M.C. and C.D. were responsible for project management for the Laboratory for Laser Energetics.

Competing interests
The authors declare no competing interests.

Additional information
Extended data is available for this paper at https://doi.org/10.1038/s41567-023-02361-4.

Correspondence and requests for materials should be addressed to V. Gopalaswamy.

Peer review information *Nature Physics* thanks Vladimir Tikhonchuk and the other, anonymous, reviewer(s) for their contribution to the peer review of this work.

Reprints and permissions information is available at www.nature.com/reprints.

https://doi.org/10.1038/s41567-023-02361-4

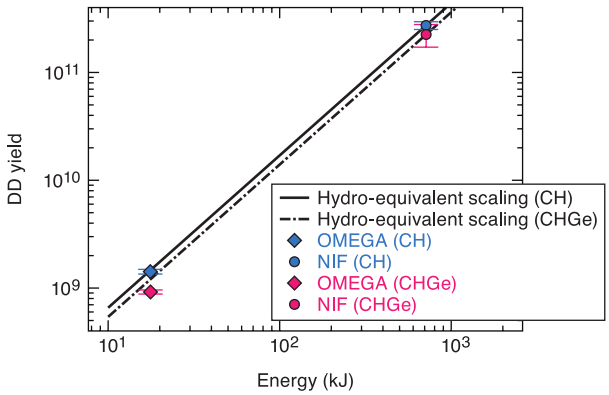

Extended Data Fig. 1 | DD fusion yields from D2 gas-filled CH ablator implosion experiments on OMEGA and NIF. DD fusion yields from D2 gas-filled CH ablator implosion experiments on OMEGA (diamonds) and NIF (circles), with (magenta) and without (blue) a Ge-doped CH inner payload layer. The black lines shows the expected yield of the NIF implosions for a range of energies according to hydro-equivalent scaling theory for the CH (solid) and CHGe (dash-dotted). The displayed yields and error bars are the median and 1 standard deviation of all the yields of implosions taken for each case, and the diagnostic measured value and 1 standard deviation uncertainty if there was only one implosion for that case. There were 4 NIF CHGe, 3 OMEGA CHGe, 2 NIF CH and 1 OMEGA CH implosions. OMEGA experiments are performed with smoothing by spectral dispersion[49] (SSD) turned off and using a polar illumination scheme[50] that mimics the illumination scheme of the NIF. OMEGA experiments occurred at 17 kJ, whereas the NIF experiments took place at 700 kJ, which corresponds to an increase in scale size S of approximate 3.5. When scaled down to OMEGA energies, the CH NIF implosions would be expected to produce $(1.42 \pm 0.12) \times 10^9$ neutrons, which is in good agreement with the $(1.42 \pm 0.07) \times 10^9$ neutrons measured on OMEGA. The CHGe NIF scaled down would be expected to produce $(1.2 \pm 0.3) \times 10^9$ neutrons, which is slightly higher than the OMEGA yields of $(8.4 \pm 0.8) \times 10^8$ neutrons. The ion temperatures for the NIF and OMEGA implosions are similar and roughly 2 keV. These implosion results support the validity of hydro-equivalent scaling of yields between OMEGA and NIF.

https://doi.org/10.1038/s41567-023-02361-4

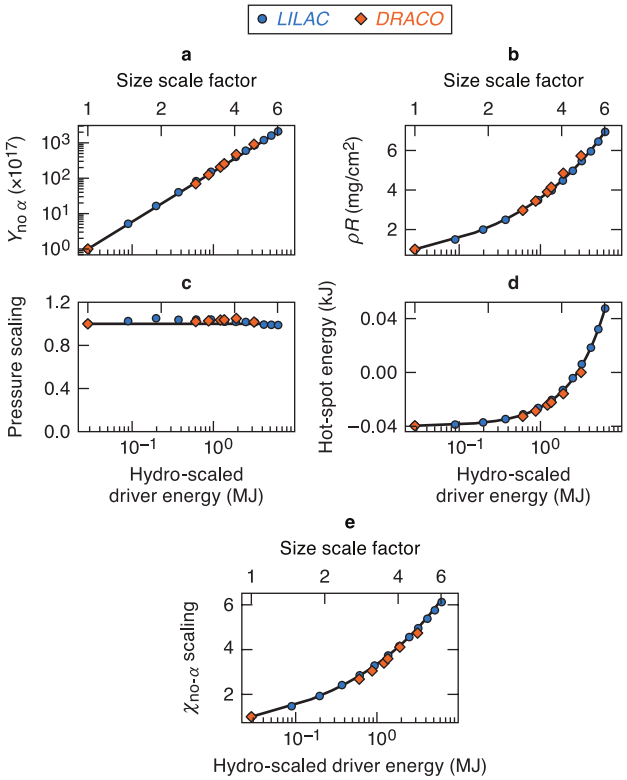

Extended Data Fig. 2 | LILAC and DRACO no-α stagnation metrics for hydro-equivalently scaled implosions. LILAC (blue circles) and DRACO (orange diamonds) no-α (that is, without alpha heating included in the simulations) stag- nation metrics for hydro-equivalently scaled implosions. a) DT Yield $Y_{no\alpha}$, b) areal density ρR, c) Pressure, d) Hotspot Energy and e) the normalized Lawson parameter $X_{no\alpha}$, all versus the hydro-equivalently scaled driver energy (lower axis) and size scale factor (upper axis). Note that both horizontal axes are logarithmic. The solid black line indicates the change in the stagnation metrics according to scaling theory in Refs. 17,18 (Extended Data Table 1). There is good agreement with scaling theory for all the key observables, indicating that the simulations have been correctly scaled, and that the scaling theory remains valid for the moderate adiabat (~ 5) implosions which are the best performers on OMEGA, even in the presence of substantial 2D perturbations as expected from prior work[48].

https://doi.org/10.1038/s41567-023-02361-4

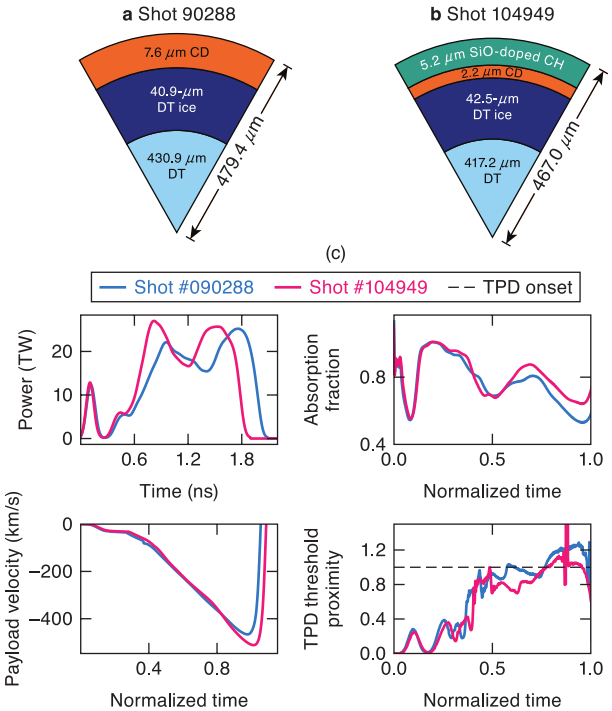

Extended Data Fig. 3 | Design changes and corresponding effect on implosion dynamics from[18] and this work. a,b) The outer section of the pure CD ablator in (a) was replaced with a 5-7% silicon-doped CH ablator, and the ice thickness was slightly increased. (c) The pulse shape and various aspects of the simulation dynamics from LILAC post-shot simulations. Shot #90288 (the highest performer from[18]) is in blue, and shot 104949 is in magenta. The pulse shape is shortened and the intensity is increased from #90288. Due to the silicon in the outer ablator, CBET is mitigated, and the higher intensity first spike has the same absorption fraction, while the fixed intensity second spike has higher absorption. This results in a substantially higher maximum velocity (from 466 to 510 km/s) for the silicon doped implosion, despite the larger mass of the ice and ablator layers. The increased temperature of the coronal plasma due to silicon also reduced the threshold parameter and activity of the two-plasmon decay (TPD).

https://doi.org/10.1038/s41567-023-02361-4

Extended Data Table 1 | Hydro-equivalent scaling coefficients for key implosion metrics

Observable	$Y_{no\alpha}$	ρR	P_{hs}	E_{hs}	$\chi_{no\alpha}$
LILAC Reconstruction of 104949	1.42	0.36	0.00	1.00	0.34
Simulations of Refs.[17, 18]	1.43	0.34	0.00	1.00	0.34
Experiments of Ref.[38]	1.42 ± 0.02				

Hydro-equivalent (HE) β from Eq. 8 based on the scaled LILAC simulations in Extended Data Figure 2, Refs. 17,18 and the experiments in Ref. 38 shown in Extended Data Figure 1. The two simulation-based methods are in agreement with each other, and the yield scaling from the experiments of Ref. 38] are in good agreement with theory. $Y_{no\alpha}$ is the DT Yield (without alpha heating), ρR is the areal density, P_{hs} is the hotspot pressure, E_{hs} is the hotspot energy, and $\chi_{no\alpha}$ is the normalized Lawson parameter.